Journal of Applied Fluid Mechanics, Vol. 8, No. 3, pp. 549-558, 2015.
Available online at www.jafmonline.net, ISSN 1735-3572, EISSN 1735-3645.
DOI: 10.18869/acadpub.jafm.67.222.19373

Lie Group Analysis for Boundary Layer Flow of Nanofluids near the Stagnation-Point over a Permeable Stretching Surface Embedded in a Porous Medium in the Presence of Radiation and Heat Generation/Absorption

P. Sreenivasulu† and N. Bhaskar Reddy

Department of Mathematics, Sri Venkateswara University, Tirupati-517502. India.

†*Corresponding Author Email: psreddysvu11@gmail.com*

(Received August 24, 2012; accepted July 21, 2014)

ABSTRACT

This study investigates the influence of thermal radiation and heat generation/absorption on a two dimensional steady boundary layer flow near the stagnation-point on a permeable stretching sheet in a porous medium saturated with nanofluids. The governing partial differential equations with the appropriate boundary conditions are reduced to a set of ordinary differential equations via Lie-group analysis. The resultant equations are then solved numerically using Runge - Kutta fourth order method along with shooting technique. Two types of nanofluids, namely, copper-water and alumina-water are considered. The velocity and temperature as well as the shear stress and heat transfer rates are computed. The influence of pertinent parameters such as radiation parameter Nr, nanofluid volume fraction parameter ϕ, the ratio of free stream velocity and stretching velocity parameter a/c , the permeability parameter K_1, suction/blowing parameter S, and heat source/sink parameter λ on the flow and heat transfer characteristics is discussed. The present study helps to understand the efficiency of heat transfer transport in nanofluids which are likely to be the smart coolants of the next generation.

Keywords: Stagnation-point flow; Porous media; Nanofluid; Stretching sheet; Scaling transformations.

NOMENCLATURE

C_f	dimensionless local Skin friction
K	permeabilty of porous medium
K_1	permeability parameter of the porous medium
k_f	thermal conductivity of base fluid
k_{nf}	thermal conductivity
k_s	thermal conductivity of nanoparticle
k^*	mean absorption coefficient
N_r	radiation parameter
Nu_x	dimensionless local Nusselt number
Pr	Prandtl number
Q_0	dimensional heat generation or absorption coefficient
q_r	radiative heat flux
Re_x	local Reynolds number
S	mass flux parameter
T	température of the nanofluid
T_∞	température of the nanofluid far from the surface
$\bar{U}(\bar{x})$	stagnation point velocity
$\bar{u},\bar{v}$	velocity components
$\bar{x},\bar{y}$	cartesian co-ordinates
α_{nf}	thermal diffusivity
λ	heat source or sink parameter
μ_{nf}	dynamic viscosity
ν_f	kinematic viscosity of the base fluid
$\bar{v}_w$	wall mass flux
ρ_{nf}	density
$(\rho C_p)_{nf}$	heat capacitance
σ^*	Stefan-Boltzmann constant
ϕ	solid volume fraction of the nanoparticles

1. INTRODUCTION

Convectional heat transfer fluids, including oil, water, and ethylene glycol mixture are poor heat transfer fluids. But the thermal conductivity of these fluids play important role on the heat transfer coefficient between the heat transfer medium and the heat transfer surface (Muthtamilselvan *et al.* 2010). In view of the rising demands of modern technology, including chemical production, power station, and microelectronics, there is a need to develop new types of fluids that will be more effective in terms of heat exchange performance. Numerous methods have been tried to improve the thermal conductivity of these fluids by suspending nano/micro-sized particle materials in liquids. Recently several researchers including Tiwari and Das (2007), Ho *et al.* (2007, 2008), Abu-Nada (2008), Oztop and Abu-Nada (2008), Abu-Nada and Oztop (2009), Congedo *et al*. (2009), Aminossadati and Ghasemi (2009), Ghasemi and Aminossadati (2009, 2010), Ahmad and Pop (2010), etc. studied on the modeling of natural convection heat transfer in nanofluids.

Hamad (2011) obtained the analytical solutions for convective flow and heat transfer of a viscous incompressible nanofluid past a semi-infinite vertical stretching sheet in the presence of magnetic field. Hamad and Pop (2011) studied the **s**caling group of transformations for boundary layer flow near the stagnation-point on a heated permeable stretching surface in a porous medium saturated with a nanofluid and heat generation/absorption effects by employing implicit finite difference technique. Khan and Pop (2010) obtained similarity solutions depending on Prandtl number, Lewis number, Brownian motion number and thermophoresis number on the steady boundary layer flow, over a stretching surface by employing implicit finite difference method. Further, Abu-Nada and Chamkha (2010) presented the natural convection heat transfer characteristics in a differentially-heated enclosure filled with a *CuO–EG–*water nanofluid for different variable thermal conductivity and variable viscosity models.

Heat, mass and momentum transfer in the laminar boundary layer flow over a stretching sheet is an important type of flow due to its application such as polymer engineering, metallurgy etc. Wang (1989) analyzed the Free convection on a vertical stretching surface by employing Runge-Kutta Fehlberg algorithm. Elbashbeshy and Bazid (2004) considered the flow and heat transfer in a porous medium over a stretching surface with internal heat generation and suction or injection. Nazar *et al*. (2004) investigated the unsteady mixed convection boundary layer flow in the region of stagnation-point on a vertical surface in a fluid-saturated porous medium. Layek *et al*. (2007) has reported heat and mass transfer boundary layer stagnation-point flow of an incompressible viscous fluid towards a heated porous stretching sheet embedded in a porous medium subject to suction/blowing with internal heat generation or absorption by employing fourth order classical Runge -Kutta method. Cortell (2005) has analyzed the effects of various physical parameters on momentum and heat transfer characteristics of the flow and heat transfer past a stretching surface in a porous medium. Malvandi *et al*. (2014), presented an HAM analysis of stagnation-point flow of nanofluid over a porous stretching sheet with heat generation.

On the other hand, the effect of radiation on boundary layer flow and heat transfer processes is of major important in the design of many advanced energy conversion systems operating at high temperatures. In view of this, Elbashbeshy and Dimian (2002) and Hossain *et al*. (1999, 2001), studied the effect of thermal radiation of a gray fluid which emits and absorbs radiation in a non-scattering medium. Elbashbeshy (2000) investigated the radiation effect on heat transfer over a stretching surface. Mukhopadyay (2009), analyzed the effects of radiation and variable fluid viscosity on flow and heat transfer along a symmetric wedge. Suneetha *et al.*(2011), studied the radiation and mass transfer effects on MHD free convective dissipative fluid in the presence of heat source/sink.

In the present paper, an attempt is made to find a similarity solution of two-dimensional stagnation point flow of an incompressible viscous radiating fluid past a porous stretching surface embedded in porous medium saturated by nanofluid, using scaling transformations.

2. MATHEMATICAL ANALYSIS

A steady laminar two-dimensional flow of an incompressible viscous radiating fluid near a stagnation-point at a porous stretching surface saturated by nanofluid is considered. The $\bar{x}$ -axis is taken along the surface and $\bar{y}$ -axis normal to it. The physical model and co-ordinate

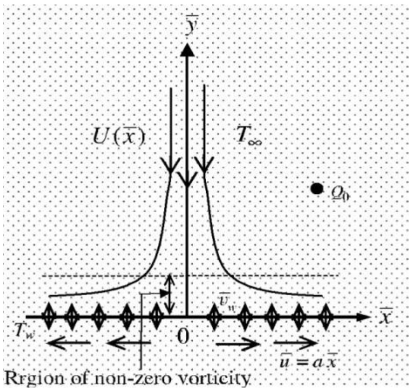

Fig. 1. Physical model and coordinate system

system is shown in Fig.1. Two equal and opposite forces are introduced along the $\bar{x}$ direction so that the wall is stretched keeping the origin fixed (Layek *et al*. 2007). It is assumed that the temperature at the stretching surface takes the constant values T_w, while the temperature of the ambient nanofluid, attained as $\bar{y}$ tends to infinity, takes the constant values T_∞. It is also assumed that the base fluid and the nanoparticles are in thermal equilibrium and no slip occurs between them. Under these assumptions and following the nanofluid model proposed by Tiwari and Das (2007), the boundary layer equations governing the flow and temperature field in the presence of radiation and heat source/sink are:

$$\frac{\partial \bar{u}}{\partial \bar{x}} + \frac{\partial \bar{v}}{\partial \bar{y}} = 0 \tag{1}$$

$$\bar{u}\frac{\partial \bar{u}}{\partial \bar{x}} + \bar{v}\frac{\partial \bar{u}}{\partial \bar{y}} = \bar{U}(\bar{x})\frac{d\bar{U}(\bar{x})}{d\bar{x}} + \frac{\mu_{nf}}{\rho_{nf}}\frac{\partial^2 \bar{u}}{\partial \bar{y}^2} + \frac{\mu_{nf}}{\rho_{nf}K}\left(\bar{U}(\bar{x}) - \bar{u}\right) \tag{2}$$

$$\bar{u}\frac{\partial T}{\partial \bar{x}} + \bar{v}\frac{\partial T}{\partial \bar{y}} = \alpha_{nf}\frac{\partial^2 T}{\partial \bar{y}^2} - \frac{1}{(\rho C_p)_{nf}}\frac{\partial q_r}{\partial \bar{y}} + \frac{Q_0}{(\rho C_p)_{nf}}(T - T_\infty) \tag{3}$$

The boundary conditions for the velocity and temperature fields are:

$$\begin{aligned} &\bar{u} = \bar{u}_w(\bar{x}) = c\bar{x},\ \bar{v} = \bar{v}_w,\ T = T_w \ \ at\ \bar{y} = 0 \\ &\bar{u} \to \bar{U}(\bar{x}) = a\bar{x},\ T \to T_\infty \ \ as\ \bar{y} \to \infty \end{aligned} \tag{4}$$

where, $\bar{x}$ and $\bar{y}$ are the coordinates along and perpendicular to the surface of the sheet, $\bar{u}$, $\bar{v}$ are the velocity components in the $\bar{x}$ and $\bar{y}$ directions, respectively, T is the local temperature of the nanofluid, $\bar{U}(\bar{x})$ stands for the stagnation-point velocity in the inviscid free stream, K is the permeability of the porous medium, q_r is the radiative heat flux, Q_0 is the dimensional heat generation or absorption coefficient, a and c are positive constants, and $\bar{v}_w$ is the wall mass flux with $\bar{v}_w$ < 0 for suctions and $\bar{v}_w$ > 0 for injection, respectively. Further, ρ_{nf} is the effective density, μ_{nf} is the effective dynamic viscosity, $(\rho C_p)_{nf}$ is the heat capacitance and α_{nf} is the effective thermal diffusivity, which are defined as (Oztop and Abu-Nada 2008; Aminossadati and Ghasemi 2009)

$$\left.\begin{aligned} &\rho_{nf} = (1-\phi)\rho_f + \phi\rho_s, \quad \mu_{nf} = \frac{\mu_f}{(1-\phi)^{2.5}} \\ &(\rho C_p)_{nf} = (1-\phi)(\rho C_p)_f + \phi(\rho C_p)_s, \\ &\alpha_{nf} = \frac{k_{nf}}{(\rho Cp)_{nf}}, \ \frac{k_{nf}}{k_f} = \frac{(k_s + 2k_f) - 2\phi(k_f - k_s)}{(k_s + 2k_f) + \phi(k_f - k_s)} \end{aligned}\right\} \tag{5}$$

where ϕ is the solid volume fraction of the nanoparticles, k_{nf} is the effective thermal conductivity of the nanofluid, k_f and k_s are the thermal conductivities of the base fluid and nanoparticle, respectively. The thermo-physical properties of the solid particles and nanofluid volume fraction are given in Table 1 (Oztop and Abu-Nada 2008).

Table 1 Thermo physical properties of fluid and nanoparticles (Oztop and Abu-Nada 2008).

Physical properties	Fluid phase (water)	Cu	Al_2o_3	Tio_3
$Cp(J/kg\,K)$	4179	385	765	686.2
$\rho(kg/m^3)$	997.1	8933	3970	4250
$k(W/m\,K)$	0.613	400	40	8.9538

By using the Rosseland approximation, the radiative heat flux is given by:

$$q_r = -\frac{4}{3}\frac{\sigma^*}{k^*}\frac{\partial T^4}{\partial \bar{y}} \tag{6}$$

where σ^* is the Stefan-Boltzmann constant and k^* is the mean absorption coefficient. It should be noted that by using the Rosseland approximation, the present analysis is limited to optically thick fluids. If the temperature differences within the flow are sufficiently small, then equation (6) can be linearized by expanding T^4 into the Taylor series about T_∞, which after neglecting higher-order terms takes the form

$$T^4 \cong 4T_\infty^3 T - 3T_\infty^4 \tag{7}$$

In view of Eqs. (6) and (7), Eq. (3) becomes:

$$\bar{u}\frac{\partial T}{\partial \bar{x}} + \bar{v}\frac{\partial T}{\partial \bar{y}} = \alpha_{nf}(1 + Nr)\frac{\partial^2 T}{\partial \bar{y}^2} + \frac{Q_0}{(\rho C_p)_{nf}}(T - T_\infty) \tag{8}$$

where $Nr = 16\sigma^* T_\infty^3 / 3k_{nf}k^*$ is the radiation parameter.

By introducing the following non-dimensional variables:

$$\begin{aligned} &x = \frac{\bar{x}}{\sqrt{\nu_f / c}}, \quad y = \frac{\bar{y}}{\sqrt{\nu_f / c}}, \quad u = \frac{\bar{u}}{\sqrt{c\nu_f}}, \\ &v = \frac{\bar{v}}{\sqrt{c\nu_f}}, U = \frac{\bar{U}}{\sqrt{c\nu_f}} \quad \theta = \frac{T - T_\infty}{T_w - T_\infty} \end{aligned} \tag{9}$$

where ν_f is the kinematic viscosity of the base fluid, Eqs. (1), (2) and (8) take the following dimensionless form:

$$\frac{\partial u}{\partial x} + \frac{\partial v}{\partial y} = 0 \tag{10}$$

$$u\frac{\partial u}{\partial x} + v\frac{\partial u}{\partial y} = U\frac{dU}{dx} + \frac{1}{(1-\phi)^{2.5}[1 - \phi + \phi(\rho_s/\rho_f)]}\left[\frac{\partial^2 u}{\partial y^2} + K_1(U - u)\right] \tag{11}$$

$$u\frac{\partial\theta}{\partial x}+v\frac{\partial\theta}{\partial y}= \frac{1}{\Pr}\frac{(1+Nr)}{[1-\phi+\phi(\rho Cp)_s/(\rho Cp)_f]}\left(\frac{k_{nf}}{k_f}\right)\frac{\partial^2\theta}{\partial y^2} +\frac{1}{\Pr}\frac{\lambda}{[1-\phi+\phi(\rho Cp)_s/(\rho Cp)_f]}\theta \tag{12}$$

The corresponding boundary conditions are:

$$u=x,\quad v=-S,\quad \theta=1\quad at\quad y=0$$
$$u\to U(x)=\frac{a}{c}x,\quad \theta\to 0\quad as\quad y\to\infty \tag{13}$$

where $\Pr=\nu_f/\alpha_f$ is the Prandtl number, $\lambda=Q_0/(\rho Cp)_f c$ is the heat source $(\lambda>0)$ or sink $(\lambda<0)$ parameter, $K_1=\nu_f/(cK)$ is the permeability parameter of the porous medium and $S=-\bar{v}_w/\sqrt{c\nu_f}$ is the mass flux parameter (S > 0 corresponds to suction and S < 0 corresponds to blowing).

By introducing the stream function ψ, which is defined by $u=\partial\psi/\partial y$ and $v=-\partial\psi/\partial x$, then the system of Eqs. (10) - (12) become:

$$\frac{\partial\psi}{\partial y}\frac{\partial^2\psi}{\partial x\partial y}-\frac{\partial\psi}{\partial x}\frac{\partial^2\psi}{\partial y^2}=U\frac{dU}{dx} +\frac{1}{(1-\phi)^{2.5}[1-\phi+\phi(\rho_s/\rho_f)]}\left\{\frac{\partial^3\psi}{\partial y^3}+K_1\left(U-\frac{\partial\psi}{\partial y}\right)\right\} \tag{14}$$

$$\frac{\partial\psi}{\partial y}\frac{\partial\theta}{\partial x}-\frac{\partial\psi}{\partial x}\frac{\partial\theta}{\partial y}= \frac{1}{\Pr}\frac{(1+Nr)}{[1-\phi+\phi(\rho Cp)_s/(\rho Cp)_f]}\left(\frac{k_{nf}}{k_f}\right)\frac{\partial^2\theta}{\partial y^2} +\frac{1}{\Pr}\frac{\lambda}{[1-\phi+\phi(\rho Cp)_s/(\rho Cp)_f]}\theta \tag{15}$$

with the boundary conditions:

$$\frac{\partial\psi}{\partial y}=x,\ \frac{\partial\psi}{\partial x}=S,\ \theta=1\ at\ y=0$$
$$\frac{\partial\psi}{\partial y}\to U=\frac{a}{c}x,\ \theta\to 0\ as\ y\to\infty \tag{16}$$

3. Scaling Transformations

We now introduce the simplified form of Lie-group transformations namely, the scaling group Γ of transformations (Ibrahim *et al.* 2005; Mukhopadhyay *et al.* 2005; Kandasamy and Muhaimin 2010; Muthtamilselvan *et al.* 2010)

$$\Gamma:\ x^*=xe^{\varepsilon\alpha_1},\ y^*=ye^{\varepsilon\alpha_2},\ \psi^*=\psi e^{\varepsilon\alpha_3},\theta^*=\theta e^{\varepsilon\alpha_4} \tag{17}$$

The one-parameter group of transformations (17) transforms the coordinates (x,y,ψ,θ) to $(x^*,y^*,\psi^*,\theta^*)$.

Substituting (17) in (14) and (15) we get,

$$e^{\varepsilon(\alpha_1+2\alpha_2-2\alpha_3)}\left(\frac{\partial\psi^*}{\partial y^*}\frac{\partial^2\psi^*}{\partial x^*\partial y^*}-\frac{\partial\psi^*}{\partial x^*}\frac{\partial^2\psi^*}{\partial y^{*2}}\right)= \frac{a^2}{c^2}e^{-\varepsilon\alpha_1}x^*+\frac{1}{(1-\phi)^{2.5}[1-\phi+\phi(\rho_s/\rho_f)]} \left\{e^{\varepsilon(3\alpha_2-\alpha_3)}\frac{\partial^3\psi^*}{\partial y^{*3}}+K_1\left(\frac{a}{c}e^{-\varepsilon\alpha_1}x^*-e^{\varepsilon(\alpha_2-\alpha_3)}\frac{\partial\psi^*}{\partial y^*}\right)\right\} \tag{18}$$

while, Eq. 15 remains invariant under the group of transformation Γ, if the following relations hold

$$\alpha_1+2\alpha_2-2\alpha_3=-\alpha_1=3\alpha_2-\alpha_3=\alpha_2-\alpha_3 \tag{19}$$

These relations give

$$\alpha_1=\alpha_3,\qquad \alpha_2=0 \tag{20}$$

Similarly, by substituting (17) into (15) and the boundary conditions (13), using (16), and from the condition that Eqs. (15) and (16) should remain invariant under the group Γ of transformations, we then obtain

$$\alpha_4=0 \tag{21}$$

The set of transformations of the Γ group reduces to

$$\Gamma: x^*=xe^{\varepsilon\alpha_1},\ y^*=y,\psi^*=\psi e^{\varepsilon\alpha_1},\theta^*=\theta \tag{22}$$

Expanding (22) in power of ε by Taylor's method and keeping terms up to the order of ε, we get

$$x^*-x=x\varepsilon\alpha_1,\quad y^*-y=0,$$
$$\psi^*-\psi=\psi\varepsilon\alpha_1,\ \theta^*-\theta=0 \tag{23}$$

The characteristic equations are:

$$\frac{dx}{x\alpha_1}=\frac{dy}{0}=\frac{d\psi}{\psi\alpha_1}=\frac{d\theta}{0} \tag{24}$$

from which, we obtain the following similarity variables

$$\eta=y,\quad \psi=xf(\eta),\quad \theta=\theta(\eta) \tag{25}$$

With the help of these relations, Eqs. (14), (15) become:

$$f_1'''+K_1\left(\frac{a}{c}-f'\right)+(1-\phi)^{2.5}\left[1-\phi+\phi(\rho_s/\rho_f)\right]\left(ff''-(f')^2+\frac{a^2}{c^2}\right)=0 \tag{26}$$

$$\frac{(1+Nr)}{\Pr}\left(\frac{k_{nf}}{k_f}\right)\theta''+[1-\phi+\phi(\rho Cp)_s/(\rho Cp)_f]f\theta'+\lambda\theta=0 \tag{27}$$

and the corresponding boundary conditions (17) become:

$$f'=1,\quad f=S,\quad \theta=1\quad at\quad \eta=0$$
$$f'\to a/c,\quad \theta\to 0\quad as\quad \eta\to\infty \tag{28}$$

where primes denotes the differentiation with respect to η. It should be observed that for a regular fluid $(\phi = 0)$ and non porous medium $(K_1 = 0)$, non permeable surface $(S = 0)$, absence of heat generation/absorption $(\lambda = 0)$ and absence of radiation $(Nr = 0)$, Eqs. (26) and (27) reduces to Eqs. (12) and (20) from the paper by Mahapatra and Gupth (2002).

The quantities of practical interest in this study are the skin friction or the shear stress co efficient C_f and the local Nusselt number Nu_x, which are defined as:

$$C_f = \frac{2\mu_{nf}}{\rho_f u_w^2}\left|\frac{\partial \bar{u}}{\partial \bar{y}}\right|_{\bar{y}=0},\ Nu_x = \frac{\bar{x}k_{nf}}{k_f(T_w - T_\infty)}\left(-\frac{\partial T}{\partial \bar{y}}\right)_{\bar{y}=0} \quad (29)$$

Using Eqs. (9), (25) and (29), the skin friction coefficient and local Nusselt number can be expressed as

$$\mathrm{Re}_x^{1/2} C_f = \frac{2}{(1-\phi)^{2.5}}\left| f''(0)\right|,\ \mathrm{Re}_x^{-1/2} Nu_x = -\frac{k_{nf}}{k_f}\theta'(0) \quad (30)$$

where $\mathrm{Re}_x = \bar{u}_w(\bar{x})\bar{x} / \nu_f$ is the local Reynolds number based on the stretching velocity $\bar{u}_w(\bar{x})$. The quantities $\mathrm{Re}_x^{1/2} C_f$ and $\mathrm{Re}_x^{-1/2} Nu_x$ are referred as the reduced skin friction coefficient and reduced local Nusselt number as in Khan and Pop (2010).

4. RESULTS AND DISCUSSION

The non linear ordinary differential equations (26) and (27) subject to the boundary conditions (28) have been solved numerically by using the Runge-Kutta fourth order method along with shooting technique. In order to validate the present results obtained by using the shooting technique, the present results are compared with that of Layek *et al.*(2007), Wang(1989), Khan and Pop(2010) and Hamad and Pop(2011) which are based on fourth order classical Runge-Kutta method, Runge-Kutta Fehlberg algorithm and Implicit Finite Difference method for appropriate reduced cases, and found that there is an excellent agreement (Tables 2, 3 and 4).

Table 2 Comparison results for $-\theta'(0)$ when $\lambda = \phi = S = a/c = K_1 = Nr = 0$

Pr	Wang (1989)	Khan and Pop (2010)	Hamad and Pop (2011)	Present results
0.07	0.0656	0.0663	0.06556	0.06576
0.2	0.1691	0.1691	0.16909	0.16952
0.7	0.4539	0.4539	0.45391	0.45392
2	0.9114	0.9113	0.91136	0.91136
7	1.8954	1.8954	1.89540	1.89540
20	3.3539	3.3539	3.39350	3.35390
70	6.46221	6.4621	6.46220	6.46220

Table 3 Comparison results for $f''(0)$ when $\lambda = \phi = S = Nr = 0, \mathrm{Pr} = 0.05$

K_1	$a/c = 2$			$a/c = 3$		
	Layek *et al.*(2007)	Hamad and Pop(2011)	Present results	Layek *et al.* (2007)	Hamad and Pop(2011)	Present results
0	1.9991	1.99907	1.99817	4.5011	4.50109	4.50218
0.1	2.0101	2.2.01021	2.01212	4.8011	4.80121	4.80312
0.5	2.1102	2.11021	2.11302	4.9102	4.91017	4.91027
1.0	2.3905	2.39018	2.39018	4.9691	4.96905	4.96918
1.5	2.7201	2.72011	2.72012	4.9901	5.00120	4.99915
2.0	3.1511	3.15120	3.15112	5.5010	5.50122	5.50125

Table 4 Comparison results for $-\theta'(0)$ when $\lambda = \phi = S = Nr = 0$

a/c	$\mathrm{Pr}=1.0$			$\mathrm{Pr}=1.5$		
	Layek *et al.* (2007)	Hamad and Pop(2011)	Present results	Layek *et al.* (2007)	Hamad and Pop(2011)	Present results
0.1	0.603	0.6072	0.602156	0.777	0.7786	0.77854
0.2	0.625	0.6216	0.624469	0.797	0.7952	0.79583
0.5	0.692	0.6937	0.693897	0.863	0.8673	0.86581
1.0	0.796	0.8001	0.798564	0.974	0.9774	0.97746
2.0	0.974	0.9788	0.997343	1.171	1.1721	1.17312
3.0	1.124	1.1221	1.124532	1.341	1.3419	1.34231

In order to bring out the salient features of the flow and the heat transfer characteristics, the numerical values for different values of the governing parameters ϕ, S, Pr, Nr, λ, a/c and K_1 are plotted in Figs.2 - 13. It is interesting to note that, no boundary layer is formed when a/c = 1.

Figures 2(a) and (b) represents the velocity $f'(\eta)$ for some values of the Cu-nanoparticle volume fraction parameter and for the values of *a/c* (= 0.1 and 2) when K_1 = 0.1, S = 0.1, $\lambda = 0.1$, and Pr = 6.8(water). It is found that the momentum boundary layer thickness decreases with an increase in ϕ, when *a/c* > 1, which implies an increase in straining motion near the stagnation-point region. Due to this reason the acceleration of the external stream is increased and this leads to thinning of the momentum boundary layer. Therefore, the existence of a nanofluid leads to a more thinning of the boundary layer. On the other hand, the flow has an inverted boundary layer structure for a/c < 1.

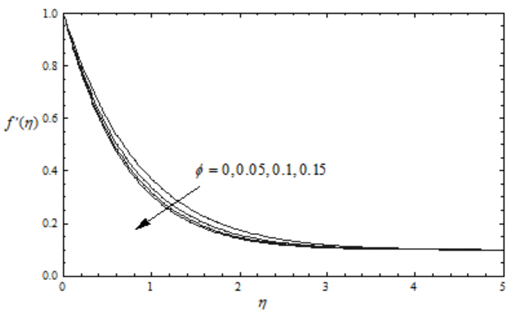

(a)

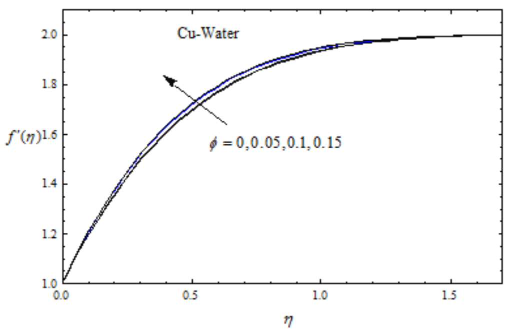

(b)

Fig. 2. Velocity profiles for different values of ϕ (a) when *a/c* = 0.1; (b) when *a/c* = 2

Figures 3(a) and (b) depict the effect of the suction/injection parameter S (< 0 for injection and > 0 for suction) for *Cu*-water on the velocity for two different values of *a/c* (= 2 and 0.1), when K_1 = 0.1 and λ = 0.1. It is seen that for *a/c* = 0.1, the effect of suction is to decrease the velocity, whereas the effect of injection is to increase the velocity. It is clear that the presence of the nanoparticles reduces the value of the velocity in both the cases of suction and injection. For *a/c* = 2, an opposite behavior is noticed.

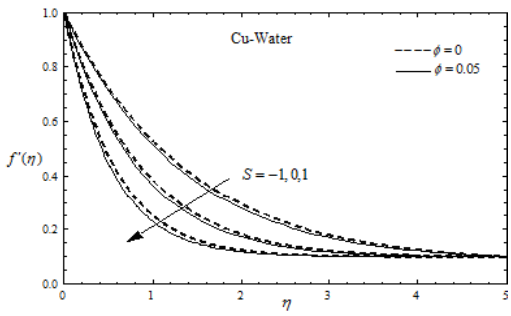

(a)

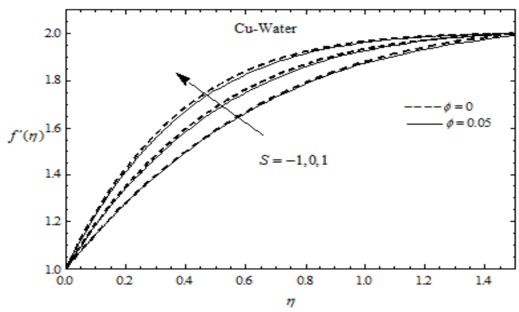

(b)

Fig. 3. Velocity profiles for different values of S (a) when *a/c* = 0.1; (b) when *a/c* = 2

The effect of Prandtl number on the velocity for both copper-water nanofluid (Pr = 2.37) and alumina-water nanofluid (Pr = 6.38) is shown in Fig.4. It is noticed that the velocity decreases as the Prandtl number increases, which shows that the velocity is higher for copper-water nanofluid than that of alumina-water nanofluid. The graphical representations of the temperature $\theta(\eta)$ for different values of the *Cu*-nanoparticle volume fraction parameter and for the values of *a/c* (= 0.1 and 2) when K_1 = 0.1, S = 0.1, λ=0.1, and Pr = 6.8 (water) is shown in Fig.5.

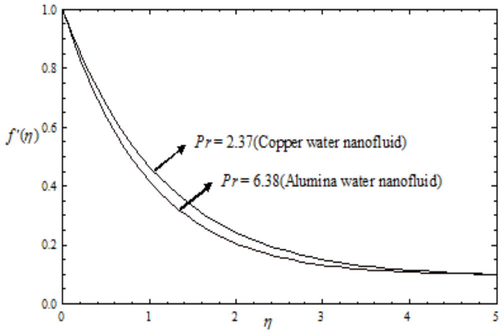

Fig. 4. Velocity profiles of copper water and alumina water nanofluid

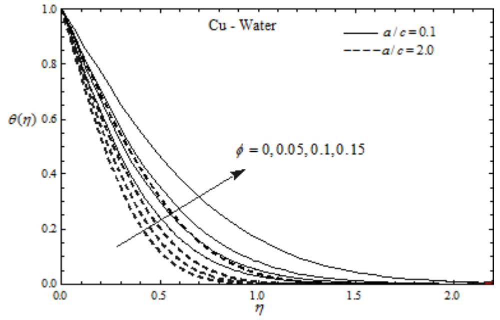

Fig. 5. Temperature profiles for different values of ϕ

It is found that the thermal boundary layer thickness for a/c < 1 is greater than for a/c > 1 and in both cases the thermal boundary layer thickness increases when the nanoparticle volume fraction parameter ϕ increases. Also, it is seen that the thermal boundary layer for Cu-water is much greater than for a regular fluid (ϕ = 0). This is because *Cu* has a higher thermal conductivity than water and the addition of it increases the thermal conductivity for the porous medium saturated with a nanofluid, so that the thickness of the thermal boundary layer increases.

Figure 6 shows the effect of the suction/injection parameter S (< 0 for injection and > 0 for suction) for Cu-water on the temperature for two different values of a/c = 2 and a/c = 0.1, when K_1 = 0.1 and λ = 0.1. It is clear that the thermal boundary layer thickness for the injection case is greater than for suction and it is much higher for *Cu*-water than for pure water (regular fluid, ϕ = 0). It is known that the effect of suction is to bring the fluid closer to the surface and, therefore, to reduce the thermal boundary layer thickness, which is evident from the Fig.6. For both the cases, the existence of *Cu* nanoparticle increases the thermal conductivity, which leads to an increase of the thickness of the thermal boundary layer. The effect of the radiation parameter on the temperature for copper-water nanofluid for two different values of a/c = 2 and a/c = 0.1, when K_1 = 0.1, S = 0.1 and λ = 0.1, is shown in Fig.7. It is observed that as the radiation parameter increases, the temperature increases for both the cases.

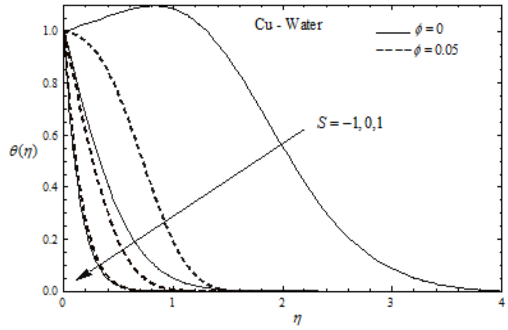

Fig. 6. Temperature profiles for different values of *S*

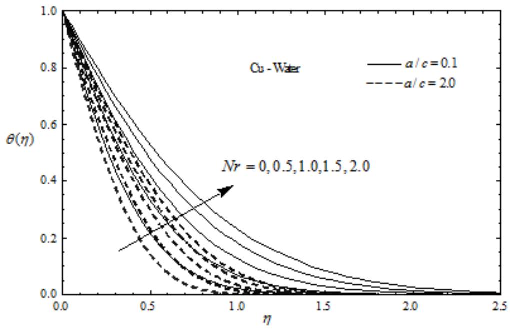

Fig. 7. Temperature profiles for different values of *Nr*

Figure 8 shows the effect of the heat generation/absorption parameter λ (< 0 for absorption and > 0 for generation) for *Cu*-water on the temperature for two different values of a/c = 2 and a/c = 0.1, when K_1 = 0.1, S = 0.1 and λ = 0.1. It is clear that the thermal boundary layer thickness for the generation case is greater than for absorption and it is much higher for *Cu*-water than for pure water (regular fluid, ϕ = 0). The effect of Prandtl number on the temperature for both copper-water nanofluid (Pr = 2.37) and alumina-water nanofluid (Pr = 6.38) is shown in Fig. 9. It is noticed that the temperature decreases as the Prandtl number increases, which shows that the temperature is higher for copper-water nanofluid than that of alumina-water nanofluid.

Figures 10 - 13 show the variation of the skin friction (shear stress) and the local Nusselt number (heat transfer rate) versus the permeability parameter K_1. It is seen from Fig. 10 that the skin friction increases with the increase of ϕ for both the cases a/c < 1 and a/c > 1. One can also see that the skin friction coefficient increases with the increase of K_1. However, it is noted from Fig. 11 that the local Nusselt number (or heat transfer rate) increases with the increase of ϕ in both the cases a/c < 1 and a/c > 1. It is found that the heat transfer rate for a/c > 1 is greater than that of for a/c < 1. Further, it is clear from Figs. 12 and 13 that both the skin friction coefficient and the local Nusselt number are greater in the case of suction than in the case of blowing. For fixed values of S and K_1, the values of the skin friction and Nusselt number for *Cu*-water are greater than for pure water (ϕ = 0). Also, it is observed that the skin friction increases while the Nusselt number decreases with the increase of K_1, in both *Cu*-water and pure water (ϕ = 0) cases.

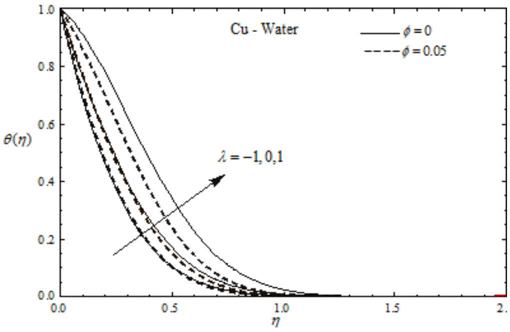

Fig. 8. Temperature profiles for different values of λ

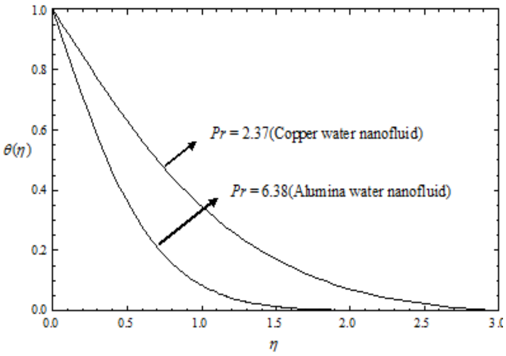

Fig. 9. Temperature profiles of copper water and alumina water nanofluid

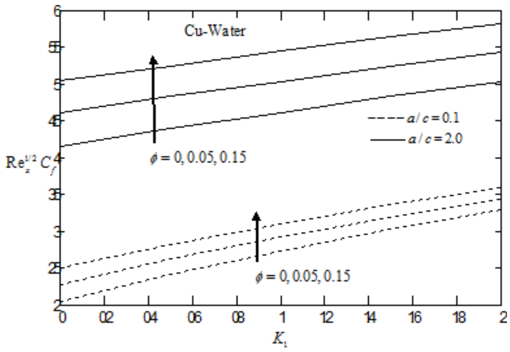

Fig. 10. Variation of the skin friction coefficient with K_1 for various ϕ

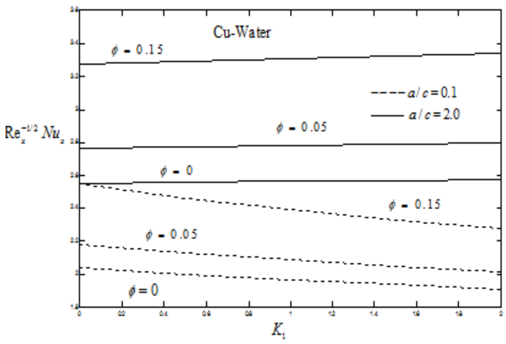

Fig. 11. Variation of local Nusselt number with K_1 for various ϕ

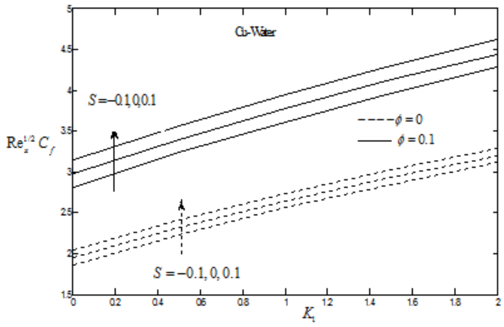

Fig. 12. Variation of the skin friction coefficient with K_1 for various S

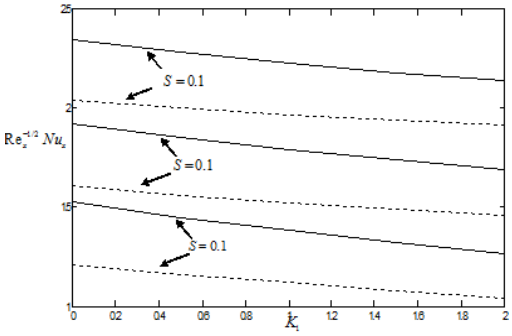

Fig. 13. Variation of the local Nusselt number with K_1 for various ϕ

5. CONCLUSIONS

The problem of two-dimensional laminar-forced convection flow over a permeable stretching surface in a porous medium saturated by a nanofluid in the presence of thermal radiation, has been studied theoretically. The model used for the nanofluid is that proposed by Tiwari and Das (2007) and very successfully used recently by several researchers. The present model finds applications in industrial cooling that could result in great energy savings and resulting emissions reductions. A set of similarity solutions is presented using Lie-group analysis. Generally in a similarity transformation, the assumed similarity variables are considered, but by using Lie-group analysis, the similarity variables can be derived directly based on the boundary conditions of the problem. The effects of the nanoparticle volume fraction parameter ϕ, permeability parameter K_1, suction/injection parameter S, heat generation/absorption parameter λ, radiation parameter Nr and the parameter a/c on the velocity and temperature, as well as the skin friction coefficient and the local Nusselt number (surface heat flux) are computed numerically for the case of pure water (Pr = 6.8). It is noticed that suction tends to stabilize the boundary layer flow and blowing can reduce the friction drag. Also it is observed that the inclusions of nanoparticles into the base fluid of this problem is capable to change the flow pattern and produces the high thermal conductivity. As it has been mentioned by Muthtamilselvan *et al*. (2010), the study of nanofluid is still at its developing stage so that it seems difficult to have a precise idea on the way the use of nanoparticles to understand the flow and heat transfer characteristics of nanofluids and identify new and unique applications for these fluids.

REFERENCES

Abu-Nada, E. (2008). Application of nanofluids for heat transfer enhancement of separated flows encountered in a backward facing step. *International Journal of Heat Fluid Flow*, 29, 242–249.

Abu-Nada, E. and A. J. Chamkha (2010). Effect of nanofluid variable properties on natural convection in enclosures filled with a CuO–EG water nanofluid. *International Journal of Thermal Sciences* 49, 2339–52.

Abu-Nada, E., and H. F. Oztop (2009). Effects of inclination angle on natural convection in enclosures filled with Cu-water nanofluid. *International Journal of Heat Fluid Flow* 30, 669 – 678.

Aminossadati, S. M. and B. Ghasemi (2009). Natural convection cooling of a localized heat source at the bottom of a nanofluid-filled enclosure. *European Journal of Mechanics - B/Fluids* 28, 630–640.

Ahmad, S. and I. Pop (2010). Mixed convection boundary layer flow from a vertical flat plate embedded in a porous medium filled with nanofluids. *International Communications in Heat and Mass Transfer* 37, 987–991.

Congedo, P. M., S. Collura, and P. M. Congedo (2009). *Modeling* and analysis of natural convection heat transfer in nanofluids. *Proceedings of ASME Summer Heat Transfer Conference*, vol. 3, 569–579.

Cortell, R. (2005). Flow and heat transfer of a fluid *through* a porous medium over a stretching surface with internal heat generation/absorption and suction/blowing. *Fluid Dynamics Research* 37, 231–245.

Elbashbeshy, E. M. A. (2000). Radiation effect on heat transfer over a stretching surface. *Canadian Journal of Physics* 78(12), 1107-1112.

Elbashbeshy, E. M. A. and M. A. A. Basid (2004). Heat transfer in a porous medium over a stretching surface with internal heat generation and suction or injection. *Applied Mathematics and Computation* 158, 799–807.

Elbashbeshy, E. M. A. and M. Dimian (2002). Effect of radiation on the flow and heat transfer over a wedge with variable viscosity. *Applied Mathematics and Computation* 132, 445-454.

Ghasemi, B. and S. M. Aminossadati (2009). Natural convection heat transfer in an inclined enclosure filled with a water-CuO nanofluid. *Numerical Heat Transfer Part A: Applications* 55, 807–823.

Ghasemi, B. and S. M. Aminossadati (2010). Periodic natural convection in a nanofluid - filled enclosure with oscillating heat flux. *International Journal of Thermal Sciences* 49, 1–9.

Hamad, M. A. A. (2011). Analytical solution of natural convection flow of a nanofluid over a linearly stretching sheet in the presence of magnetic field, *International Communication in Heat and Mass Transfer* 38, 487–92.

Hamad, M. A. A. and I. Pop (2011). Scaling Transformations for Boundary Layer Flow near the *Stagnation*-Point on a Heated Permeable Stretching Surface in a Porous Medium Saturated with a Nanofluid and Heat Generation/Absorption Effects. *Transport in Porous Media* 87, 25-39.

Ho, C. J., M. W. Chen, and Z. W. Li (2007). Effect of natural convection heat transfer of nanofluid in an enclosure due to uncertainties of viscosity and thermal conductivity. *In Proceedings of ASME/JSME Thermal Engineering.Summer Heat Transfer Conference—HT* 1, 833–841.

Ho, C. J., M. W. Chen, and Z. W. Li (2008). Numerical simulation of natural convection of nanofluid in a square enclosure: Effects due to uncertainties of viscosity and thermal conductivity. *International Journal in Heat Mass Transfer*. 51, 4506–4516.

Hossain, M. A., M. A. Alim, and D. Rees (1999). *Effect* of radiation on free convection from a porous vertical plate. *International Journal in Heat Mass Transfer*. 42, 181-191.

Hossain, M. A., K. Khanafer, and K. Vafai (2001). Effect of *radiation* on free convection flow of fluid with variable viscosity from a porous vertical plate. *International Journal of Thermal Sciences* 40, 115-124.

Ibrahim, F. S., M. A. Mansour, and M. A. A. Hamad (2005). Lie-groupanalysis of radiation and magnetic field effects on free convection and mass transfer flow past a semi-infinite vertical flat plate. *Electronic Journal of Differential Equations*, 1–17.

Kandasamy, R., and I. Muhaimin (2010). Scaling transformation for the effect of temperature-dependent fluid viscosity with thermophoresis particle deposition on MHD free convection heat and mass transfer over a porous stretching surface. *Transport Porous Media* 84, 549–568.

Khan, W. A. and I. Pop (2010). Boundary-layer flow of a nanofluid past a stretching sheet. *International* Journal *of Heat Mass Transfer* 53, 2477–83.

Layek, G. C., S. Mukhopadhyay, and S. A. Samad (2007). Heat and mass transfer analysis for boundary layer stagnation-point flow towards a heated porous stretching sheet with heat absorption/generation and suction/blowing. *International Communication in Heat MassTransfer* 34, 347–56.

Mahapatra, T. R. and Gupta, A. S. (2002). Heat transfer in stagnation-point flow towards a stretching sheet. *Heat Mass Transfer* 38, 517–521.

Malvandi, A., F. Hedayati, and M. R. H Nobari (2014). An HAM analysis of stagnation-point flow of nanofluid over a porous stretching sheet with heat generation, *Journal of Applied Fluid Mechanics* 7(1), 135-145.

Muthtamilselvan, M., P. Kandaswamy, and J. Lee (2010). Heat transfer enhancement of copper-water nanofluids in a lid-driven enclosure. *Communications in Nonlinear Science and Numerical Simulation* 15, 1501–510.

Mukhopadyaya, S. (2009). Effects of Radiation and Variable Fluid Viscosity on Flow and Heat Transfer along a Symmetric Wedge. *Journal of Applied Fluid Mechanics* 2(2), 29-34.

Mukhopadhyay, S., G. C. Layek, and S.A. Samad (2005). Study of MHD boundary layer flow over a heated stretching sheet with variable viscosity. *International Journal of Heat and Mass Transfer* 48, 4460–4466.

Nazar, R., N. Amin, D. Filip, and I. Pop (2004). Unsteady boundary layer flow in the region of the stagnation-point on a stretching sheet. *International Journal of Engineering Science* 42, 1241–53.

Oztop, H. F. and E. Abu-Nada (2008). Numerical study of natural convection in partially heated rectangular enclosures filled with nanofluids. *International Journal of Heat and Fluid Flow* 29, 1326–1336.

Suneetha, S., N. Bhaskar Reddy, and V. Ramachandra Prasad (2011). Radiation and mass transfer effects on MHD free convective dissipative fluid in the presence of heat source/sink. *Journal of Applied Fluid Mechanics* 4(1), 107-113.

Tiwari, R. K., and M. K. Das (2007). Heat transfer augmentation in a two-sided lid-driven differentially heated square cavity utilizing nanofluids. *International Journal of Heat and Mass Transfer* 50, 2002–2018.

Wang, C. Y. (1989). Free convection on a vertical stretching surface. *Journal of Applied Mathematics and Mechanics* 69, 418–420.